CHEMISTRY OF MATERIALS

pubs.acs.org/cm

Article

# Correlating ZnSe Quantum Dot Absorption with Particle Size and Concentration

Reyhaneh Toufanian, Xingjian Zhong, Joshua C. Kays, Alexander M. Saeboe, and Allison M. Dennis*

Cite This: *Chem. Mater.* 2021, 33, 7527−7536

Read Online

ACCESS | Metrics & More | Article Recommendations | Supporting Information

**ABSTRACT:** The focus on heavy metal-free semiconductor nanocrystals has increased interest in ZnSe semiconductor quantum dots (QDs) over the past decade. Reliable and consistent incorporation of ZnSe cores into core/shell heterostructures or devices requires empirical fit equations correlating the lowest-energy electron transition (1S peak) to their size and molar extinction coefficients ($\varepsilon$). While these equations are known and heavily used for CdSe, CdTe, CdS, PbS, etc., they are not well established for ZnSe and are nonexistent for ZnSe QDs with diameters <3.5 nm. In this study, a series of ZnSe QDs with diameters ranging from 2 to 6 nm were characterized by small-angle X-ray scattering (SAXS), transmission electron microscopy (TEM), UV−vis spectroscopy, and microwave plasma atomic emission spectroscopy (MP-AES). SAXS-based size analysis enabled the practical inclusion of small particles in the evaluation, and elemental analysis with MP-AES elucidates a nonstoichiometric Zn:Se ratio consistent with zinc-terminated spherical ZnSe QDs. Using these combined results, empirical fit equations correlating QD size with its lowest-energy electron transition (i.e., 1S peak position), Zn:Se ratio, and molar extinction coefficients for 1S peak, 1S integral, and high-energy wavelengths are reported. Finally, the equations are used to track the evolution of a ZnSe core reaction. These results will enable the consistent and reliable use of ZnSe core particles in complex heterostructures and devices.

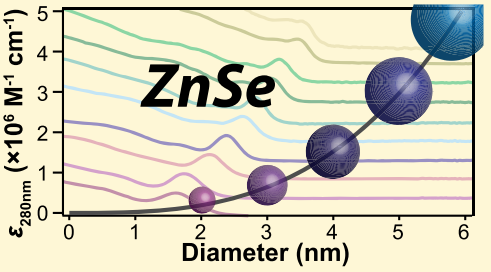




The unique photophysical properties of semiconductor quantum dots (QDs) arise as the quantum confinement of excited electrons produces precisely tuned size-dependent optoelectronic properties. Their color tunability, narrow emission spectra, high quantum yield, and chemical and photostability have resulted in their extensive use in optoelectronic devices,[1−3] as well as in biosensing and biomedical imaging applications.[4−6] As the application of QDs grows in mass-produced consumer electronics and sensitive biological applications, interest in heavy metal-free compositions increases as well. With a bulk band gap of 460 nm (2.7 eV), colloidal ZnSe-based QDs are a leading candidate for the fabrication of violet and blue LEDs, displays, and laser diodes, making the synthetic development of these nanoparticles technologically important.[3,7−9] In this context, ZnSe QDs have been used in the development of more complex nanomaterials including ZnSe/ZnS core/shell heterostructures,[7] ZnSeTe-alloyed QDs,[10] and Cu- or Mn-doped ZnSe/ZnS QDs.[11,12]

To precisely fabricate QD-containing devices or synthesize complex nanostructures,[13] it is necessary to know the core QD size and concentration in solution. Empirical fit equations correlating the position of the lowest-energy electron transition (1S peak) to the QD size and its molar extinction coefficient ($\varepsilon_{1S}$) are often used to quickly, economically, and nondestructively characterize QD samples.[14] These equations are derived by combining UV−vis absorption spectra with sizing data obtained from transmission electron microscopy (TEM) images and elemental concentrations determined by mass spectroscopy, respectively. With known molar extinction coefficients at either the 1S peak or high-energy wavelengths outside the quantum confinement regime,[15] one can use the Beer−Lambert law to calculate QD concentration. While these empirical fit equations are known and heavily used for semiconductors such as CdSe,[16] CdS,[16] CdTe,[16] PbS,[17] and PbSe,[15] there were no reports elaborating on the size and molar extinction coefficient relationship for ZnSe nanocrystals until recently.[18] Given the limited range of ZnSe particle sizes in the previous report and the nonphysical nature of the fitting equations outside this range, we expand upon these results by examining a larger range of particle sizes. In this study, in addition to relating the 1S peak and QD size, we determined empirical equations correlating the 1S peak height, the area under the 1S peak, and high-energy absorption measurements to ZnSe concentration.

ZnSe QDs have been synthesized using a variety of routes including arrested precipitation,[19] reverse micelle,[20] heat-up,[21] and hot-injection methods.[22] Here, monodisperse ZnSe

Received: July 19, 2021
Published: September 16, 2021

nanocrystals between 2 and 6 nm in diameter were synthesized by combining a hot-injection method and the extended LaMer model of growth *via* a continuous drip injection.[23] In this reaction, a burst of nucleation takes place due to precursor supersaturation following the rapid injection of diethyl zinc ($Et_2Zn$) into a mixture of oleylamine and trioctylphosphine:-selenide at 300 °C. Nanoparticle growth proceeds through a continuous drip addition of the cationic and anionic precursors at the same temperature. Control of the reaction time, and therefore the volume of precursors added into the reaction solution, results in the formation of ZnSe QDs of different sizes. Particle growth was monitored by taking absorbance measurements of diluted samples and tracking the position of the 1S peak as it shifted from 361 nm to 422 nm (Figure 1).

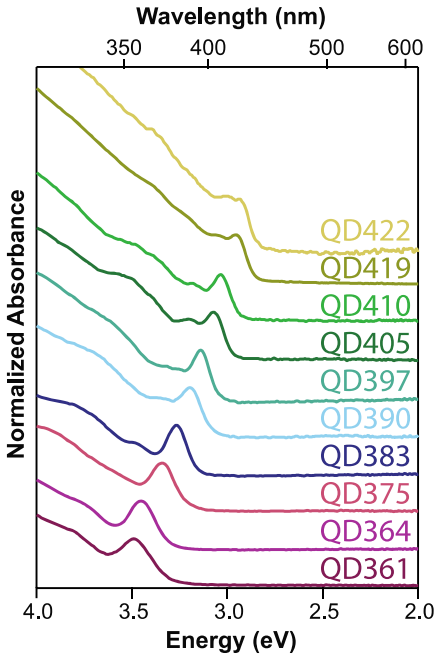


**Figure 1.** UV−vis spectroscopy of ZnSe cores. 1S peak-normalized absorbance spectra of ZnSe core QDs with 1S peaks between 361 and 422 nm.

For each QD sample, the reaction was ceased by removing the flask from the heating mantle and placing it on an aluminum block to rapidly cool to room temperature. Each sample was named to correspond with the resulting 1S peak position (e.g., QD361 and QD422).

Powder X-ray diffraction (XRD) measurements performed on QD394 and QD423 confirmed their zinc-blende crystal structure (Figure 2a). The peak positions of the nanocrystals at 26.9, 44.6, and 52.9 degrees correspond to the (111), (220), and (311) crystal planes and are consistent with previously reported ZnSe nanocrystals synthesized using phosphine−selenium precursors.[24,25] A narrowing of the XRD peaks is observed in the spectra obtained from QD422 compared with that from QD397, consistent with an increase in the nanoparticle diameter. For the determination of average particle diameters, synthesized nanocrystals were imaged using transmission electron microscopy (TEM), where lattice fringes are visible throughout the nanocrystals, further demonstrating their crystallinity (Figure 2). Average diameters were calculated by measuring the area enclosed within each

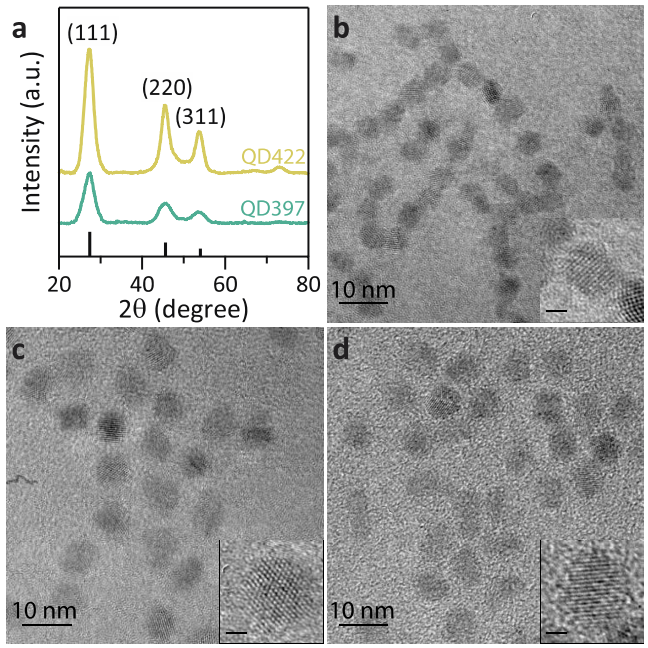


**Figure 2.** Structure and morphology of ZnSe core particles. (a) XRD spectra of QD397 and QD422 along with reference peaks for zinc-blende ZnSe from the database described in ref 26.[26] Size-matched TEM images of (b) QD405, (c) QD419, and (d) QD422. The scale bar indicates 10 nm, and the inset in each image depicts a 10 nm × 10 nm area with a scale bar of 2 nm.

nanocrystal and assuming a spherical morphology ($n$ = 126−236 QDs per QD sample; Figures S1 and S2).

While TEM is a valuable tool for obtaining essential morphological and crystallographic information, limitations arise in obtaining reliable sizing information of nanocrystals. The number of nanocrystals imaged is often not representative of the entire sample: while a QD suspension contains billions of nanoparticles, usually only a few hundred QDs are imaged and sized.[27] In addition, the low contrast of semiconductor QDs compared to background, especially in the case of heavy metal-free QDs such as ZnSe and InP, inhibits the utility of the automated sizing of QDs, necessitating manual sizing of individual QDs. This adds individual errors and person-to-person variability to the uncertainty of the sizing results, especially for QDs < 4 nm in diameter. Therefore, small-angle X-ray scattering (SAXS) can be used as an additional or alternative sizing tool.[27,28] Suspensions of as-synthesized QDs were diluted with hexanes and loaded into quartz capillaries, enabling ensemble sizing measurements on a significantly larger sample size without risk of size-selective precipitation biasing the sizing results.

The SAXS data were modeled using a spherical form factor and assuming a log−normal size distribution (Figure 3a). The reaction solution does not affect the measured average diameters, as a direct comparison of an as-synthesized aliquot and a purified solution of QD422 yields identical diameters: 5.77 ± 0.94 and 5.74 ± 0.98 nm, respectively (Figure S3). The same measurement was also modeled as a spherical core/shell heterostructure to distinguish between the contribution of ZnSe cores and surface ligands. In this case, the core diameter was the same (5.74 ± 0.98) and the model yielded a negligible shell thickness. This confirms that the presence of ligands on the surface of the particles or in the reaction solution does not


https://doi.org/10.1021/acs.chemmater.1c02501
Chem. Mater. 2021, 33, 7527−7536

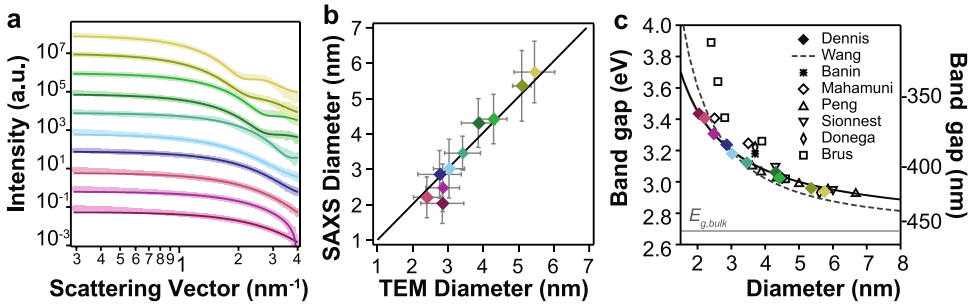


**Figure 3.** Sizing analysis of ZnSe QDs. (a) Experimental SAXS patterns for ZnSe QDs, fitted with a log−normal size distribution to a spherical model (lines). (b) Comparison of particle diameters obtained using SAXS and TEM. The black line denotes an empirical fit with a slope of 1.01, $R^2$ = 0.99. (c) Relationship between the SAXS diameters and band gap, as determined from the 1S peak position. Data from previously published ZnSe cores included for comparison,[18,19,30−33] along with a previously published theoretical equation for the relationship between ZnSe core size and band-gap energy (dashed line).[34] The solid black line indicates the fit equation to the data original to this publication (solid diamonds). The colors and sample ordering used in this figure are consistent with the colors and labels in Figure 1.

contribute to the measured diameters, consistent with similar studies performed on PbS QDs in the presence of oleic acid.[29]

To confirm the accuracy of SAXS as an alternative sizing method for small-diameter nanoparticles, we compared sizing data obtained from SAXS and TEM; the slope of the line (SAXS diameter = slope · TEM diameter) relating the two measurements is 1.01 ± 0.03, indicating strong agreement between the two sizing approaches (Figure 3b). While we observe that the standard deviations of measurements performed through SAXS are larger than those obtained via TEM, the trends in the SAXS means are more consistent with those seen for the optical band gaps at small particle sizes (Table S1). Specifically, for the smallest particles, the TEM sizes do not increase monotonically with larger 1S peak wavelengths, whereas this subtle size differentiation is discernible in the SAXS mean diameters (Figure S4). Thus, we chose to use the SAXS measurements for our subsequent analysis.

The 1S peak positions (band gaps) are plotted against their corresponding average diameters in Figure 3c (filled, colored markers) and compared to literature reports (Figure 3c, open black markers). Our sizing data are in agreement with the theoretical work of Wang et al. (dashed line).[34] Notably, the correlation between the 1S peak position and SAXS diameters also fits the previously published data on wurtzite ZnSe QDs, which exhibit 1S peaks at 390 and 420 nm for QDs of 3.0 and 4.7 nm diameters, respectively.[35] A simple empirical fit equation adjusts the ZnSe band gap (2.70 eV) for the size-based quantum confinement by correlating the energy of the first electronic transition ($E_{1S}$, eV) with diameter ($D$, nm)

$$E_{1S}\ (\text{eV}) = 2.70 + \frac{1.46}{D},\quad X^2 = 0.999 \tag{1}$$

Typically, the adjustment for confinement also includes a $D^2$ term in the denominator, but we found the contribution from this term in this size regime to be negligible, consistent with observations made for lead-based chalcogenides (i.e., PbS, PbSe, and PbTe).[15,17,36]

To easily use experimental absorbance spectra to determine the size of particles in a solution, a second fitting equation efficiently relates the difference between the bulk band gap of ZnSe (460 nm) and 1S peak position ($\lambda$, nm) to the particle diameter ($D$, nm) (Figure 4a)

$$D\ (\text{nm}) = \frac{215}{(459 - \lambda_{1S})},\quad X^2 = 0.999 \tag{2}$$

We note that during the preparation of this paper, another report on the size and molar extinction coefficient of ZnSe QDs with 1S peaks in the range of 400−424 nm was published, wherein a greater focus was placed on the surface properties of

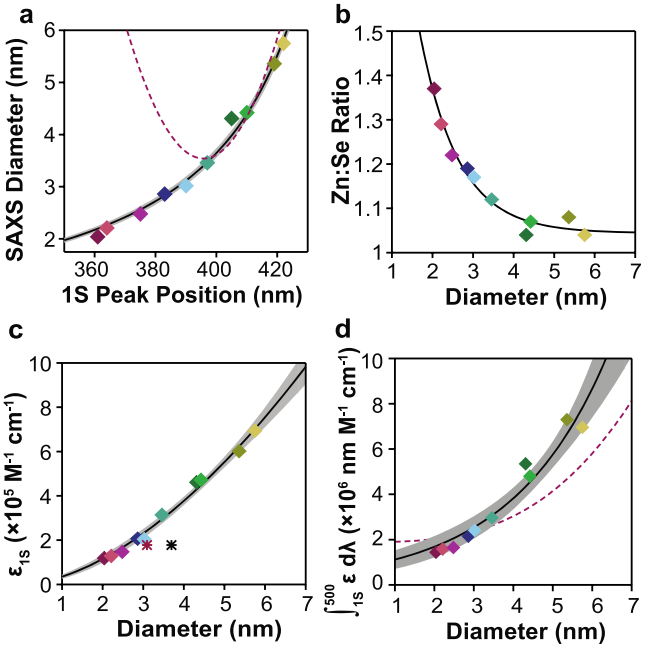


**Figure 4.** Size-dependent characterization of ZnSe particles. (a) Diameter versus first exciton absorption (1S) peak position. (b) Plot of the ratio of zinc and selenium versus diameter indicates that smaller particles exhibit a larger excess of zinc atoms due to zinc atoms on the particle surface. (c) ZnSe QD at the 1S peak position as a function of particle size. The black asterisk represents the data point from Banin et al., using their reported 3.7 nm diameter; the reported 390 nm 1S peak for this particle indicates a 3.1 nm diameter by our sizing analysis, as presented by the red asterisk.[30] (d) Integrated ZnSe QD molar extinction coefficient taken by integrating from the 1S peak wavelength to 500 nm. In each plot, the black line indicates a fit function with the 95% confidence interval shaded in light gray. The dotted lines in panels (a) and (d) are the fit function from Peng et al., which was fit using data with first exciton absorption peaks ranging from 400 to 422 nm.[18]



https://doi.org/10.1021/acs.chemmater.1c02501
Chem. Mater. 2021, 33, 7527−7536

**Table 1. Summary of MP-AES Data**

| sample[a] | diameter (nm)[b] | $C_{Zn}$ (mg/L) | $C_{Se}$ (mg/L) | no. of atoms (A) | Zn/Se molar ratio ($R_{Zn/Se}$) | $\varepsilon_{1S}$ ($10^5$ $M^{-1}$ $cm^{-1}$) | $\int_{1S}^{500} \varepsilon\, d\lambda$ ($10^6$ nm $M^{-1}$ $cm^{-1}$) |
|---|---|---|---|---|---|---|---|
| QD361 | 2.04 ± 0.57 | 33.89 | 30.11 | 195 | 1.36 | 1.19 | 1.44 |
| QD364 | 2.21 ± 0.58 | 40.79 | 38.34 | 248 | 1.29 | 1.29 | 1.58 |
| QD375 | 2.48 ± 0.67 | 42.70 | 42.27 | 351 | 1.22 | 1.47 | 1.65 |
| QD383 | 2.86 ± 0.67 | 46.24 | 46.76 | 538 | 1.19 | 2.06 | 2.15 |
| QD390 | 3.02 ± 0.83 | 41.30 | 42.73 | 633 | 1.17 | 2.04 | 2.41 |
| QD397 | 3.46 ± 0.48 | 42.16 | 45.29 | 952 | 1.12 | 3.14 | 2.96 |
| QD405 | 4.31 ± 0.69 | 40.43 | 46.92 | 1840 | 1.04 | 4.61 | 5.35 |
| QD410 | 4.42 ± 0.70 | 41.34 | 46.61 | 1984 | 1.07 | 4.72 | 4.80 |
| QD419 | 5.36 ± 1.00 | 40.66 | 45.62 | 3539 | 1.08 | 6.02 | 7.30 |
| QD422 | 5.75 ± 0.87 | 41.32 | 47.95 | 4369 | 1.04 | 6.94 | 6.96 |

[a]Sample nomenclature indicates the 1S absorption peak position. [b]Reported diameters are means ± standard deviation (SD) of SAXS measurements. SD = PDI/$r$, where PDI is the measurement polydispersity index and $r$ is the average radius of the sample.

the QDs.[18] Our experiments expand this range to QDs with 1S peaks ranging from 361 to 422 nm, which results in empirical fit equations covering a broader range of QD diameters and optical properties. The benefits of the broader range of particles and the new fitting function are seen in Figure 4a, where the previously published quadratic sizing equation (dashed line) fits our data well over the previous sample range of 400−424 nm but rapidly diverges outside that range. The form of eq 2 is physically consistent with the nature of the quantum dot confinement-based change in band gap, meaning that there is less of a risk of substantial deviations from the fitting equation outside the range of the experimental data used to generate the fit. This can be particularly important when the equations are disseminated for broad use without noting the valid range of 1S peaks for application.

While there are several published experimental and theoretical values relating the 1S peak position to average nanocrystal diameters for ZnSe QDs, there are currently only two reports of its molar extinction coefficient in the literature: Banin et al. report a molar extinction coefficient of 180 000 $M^{-1}$ $cm^{-1}$ for ZnSe QDs with a 1S peak at 390 nm and a reported diameter of 3.7 nm,[30] while Peng et al.[18] recently reported integrated molar extinction coefficient values for ZnSe QDs with an empirical fit equation valid for particles with 1S peaks ranging from 400 to 424 nm.

Molar extinction coefficients can be empirically determined by carefully correlating the absorbance of a sample of QDs with known size with the concentration of its constituents using elemental analysis. To this end, each QD sample was purified through precipitation with ethanol and its absorbance in hexane was carefully measured before the sample was dried under vacuum and acid-digested for analysis using microwave plasma atomic emission spectrometry (MP-AES). QDs of different sizes do not necessarily have equimolar ratios of cation to anion.[15,37] Thus, assuming a 1:1 cation:anion ratio can skew the molar extinction coefficient values and obtaining precise counts of both cations and anions in each QD sample is essential to the accurate calculation of molar extinction coefficients. This becomes challenging for QD compositions comprising Se. In a recent study, Morrison et al. reported that exposure of selenium to nitric acid results in the formation of the $H_2Se$ gas, compromising the accuracy of the measurements. It was noted that preoxidizing the samples with hydrogen peroxide ($H_2O_2$) can mitigate the formation of volatile compounds upon the addition of a strong acid.[38] The same approach was used here to digest the ZnSe size series, whereby each QD sample was first oxidized using $H_2O_2$ prior to digestion with nitric acid. In addition, since many elements adsorb to the surface of borosilicate glass, its use in any phase of the analysis was avoided. The digestion was performed in polypropylene centrifuge tubes, which are resistant to both strong acids and oxidizers.[38]

The concentration of each QD suspension was calculated using sizing data obtained via SAXS measurements, and the number of Zn and Se ions was calculated via elemental analysis. Specifically, the molar ratios were calculated using the weight concentration of each ion ($C_{Zn}$ and $C_{Se}$, mg/L) and accounting for their corresponding molar masses ($M_{Zn}$ = 65.38 g/mol and $M_{Se}$ = 78.97 g/mol)

$$R_{Zn/Se} = \frac{C_{Zn} M_{Se}}{C_{Se} M_{Zn}} \tag{3}$$

Table 1 summarizes the MP-AES data obtained for each QD sample. The Zn:Se molar ratios ($R_{Zn/Se}$) obtained by MP-AES are nonstoichiometric (Figure 4b), consistent with those reported for PbSe and PbS QDs.[15,17] $R_{Zn/Se}$ decreases with increasing diameter, with all samples exhibiting an excess of zinc ions, consistent with similar reports of cation-terminated spherical QDs.[15] The size-dependent $R_{Zn/Se}$ is well described by an exponential function that asymptotes at an even distribution of the elemental components (i.e., $\lim_{D\to\infty} R_{Zn/Se} = 1$)

$$R_{(Zn/Se)} = 1 + 1.58D^{(-2.09)},\ X^2 = 0.999 \tag{4}$$

Assuming a spherical nanocrystal, the total number of atoms in each QD is related to its diameter ($D$) and the ZnSe lattice constant ($a$ = 0.567 nm)

$$N = \frac{4\pi}{3}\left(\frac{D}{a}\right)^3 \tag{5}$$

The QD concentration ($C_{QD}$, M) was calculated from the measured Zn and Se mass concentrations ($C_{Zn}$ and $C_{Se}$, respectively) and the number of atoms in the particle

$$C_{QD} = \frac{10^{-3}}{N}\left(\frac{C_{Zn}}{M_{Zn}} + \frac{C_{Se}}{M_{Se}}\right) \tag{6}$$

This particle concentration was combined with the carefully measured absorbance spectra from the same samples to calculate the molar extinction coefficient at the 1S peak using the Beer−Lambert law. With the 1S peak molar extinction coefficient ($\varepsilon_{1S}$, $M^{-1}$ $cm^{-1}$) calculated for each sample, the correlation between the nanocrystal diameter ($D$, nm) and the


https://doi.org/10.1021/acs.chemmater.1c02501
Chem. Mater. 2021, 33, 7527−7536

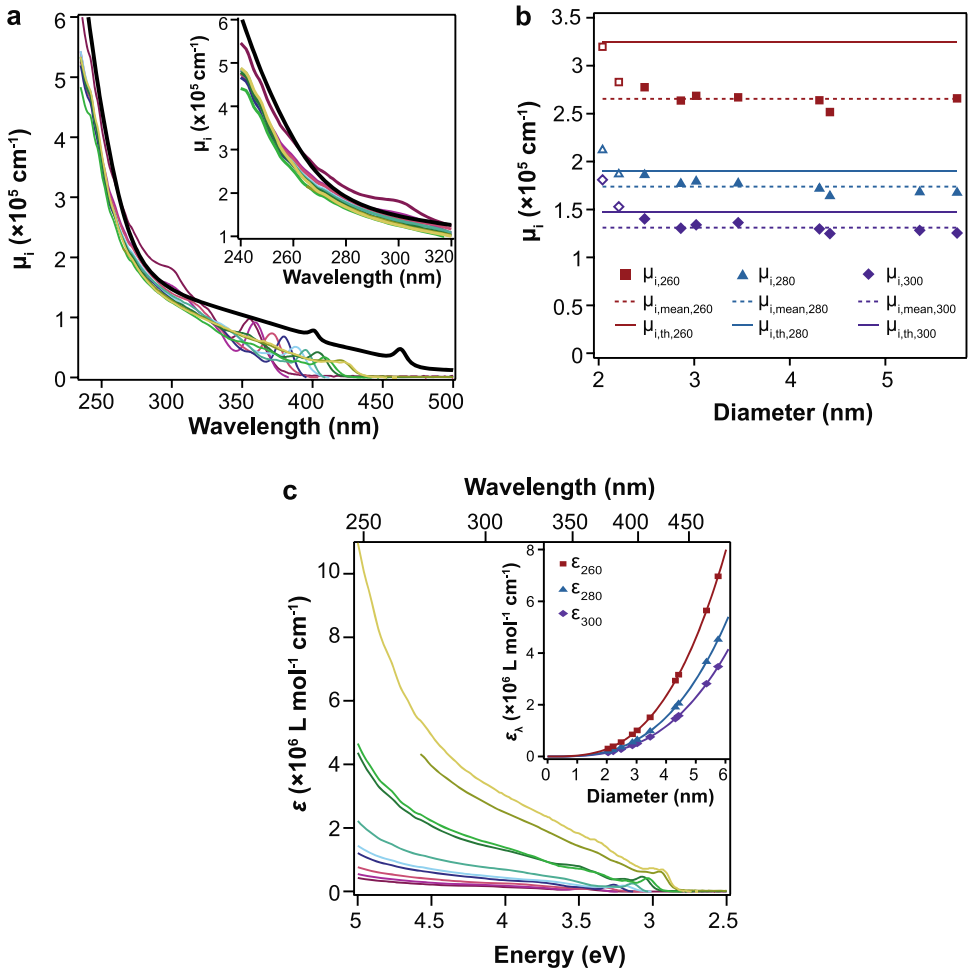


**Figure 5.** High-energy absorption analysis of ZnSe particles. (a) Intrinsic absorption coefficient ($\mu_i$) spectra for 10 experimental samples (colored lines) in hexane and the theoretically calculated bulk intrinsic absorption coefficient ($\mu_{i,th}$) for ZnSe in hexane (thick black line). A zoomed-in region (inset) shows where the experimental and bulk values largely coincide at high-energy wavelengths. (b) Intrinsic absorption coefficient ($\mu_i$) at 260, 280, and 300 nm of ZnSe QDs of a range of sizes (squares, triangles, and diamonds, respectively) as well as $\mu_{i,th}$ (solid lines) and mean values $\mu_{i,mean}$ (dashed lines) at the same wavelengths. The two smallest particles are excluded from the calculation of $\mu_{i,mean}$ because they exhibit quantum confinement effects at the relevant wavelengths and are thus depicted with open shapes in contrast to the solid shapes used for the included values. (c) Molar extinction coefficient ($\varepsilon$) spectra of a size series of ZnSe QDs. Inset: plots of the molar extinction coefficients of the ZnSe QDs at 260, 280, and 300 nm versus particle diameter show the correlation between molar extinction coefficient and particle volume. The lines show the best fits to a $D^3$ power law.

corresponding molar extinction coefficient was fit to a power law equation (Figure 4c)

$$\varepsilon_{1S} = 35\ 100 \cdot D^{1.71},\ X^2 = 0.999 \quad (7)$$

This power is on par with the $\propto D^{1.85}$ power reported for both zinc-blende CdS and CdSe.[39]

Because the 1S peak becomes wider and flatter (lower intensity at its peak) as the particle size dispersity increases, using the 1S peak intensity to calculate concentration can underestimate the concentration of polydisperse QD samples. As an alternative, the integrated 1S peak can be used to calculate the molar extinction coefficient by capturing the contribution of the breadth of the 1S peak. In this case, the molar extinction coefficient is integrated from the 1S peak to 500 nm to capture the lowest-excited-state absorption with minimal contribution from other absorption bands (Figure 4d). The relationship between zinc-capped ZnSe QDs and the integrated molar extinction coefficient has been previously described as the sum of a QD volume ($D^3$) term related to the bulk contribution and an exponential term for quantum confinement.[18] In our assessment of both the previous data and our own, we found that the $D^3$ term contributes minimally to the shape of the fitting curve, enabling the exponential term alone to be used to describe the relationship between the particle size and the integrated molar extinction coefficient

$$\int_{1S}^{500\ \mathrm{nm}} \varepsilon\ \mathrm{d}\lambda = 744\ 000 \exp\left(\frac{D}{2.44}\right),\ X^2 = 0.900 \quad (8)$$

Although the integrated molar extinction coefficient alleviates error arising from the polydispersity of the sample, the precise choice of the 1S peak value introduces another source of variability. Because the region around the 1S peak has the highest absorbance values of the integrated range, the shift of a couple of nm higher or lower in the 1S peak determination can noticeably increase or decrease the integrated absorbance.

As an alternative to the 1S peak-based approaches, high-energy absorption measurements can be used with a size-independent intrinsic absorption coefficient ($\mu_i$) or molar extinction coefficient ($\varepsilon$) to calculate the total concentration of semiconductor units or particles of known diameter in a


https://doi.org/10.1021/acs.chemmater.1c02501
Chem. Mater. 2021, 33, 7527−7536

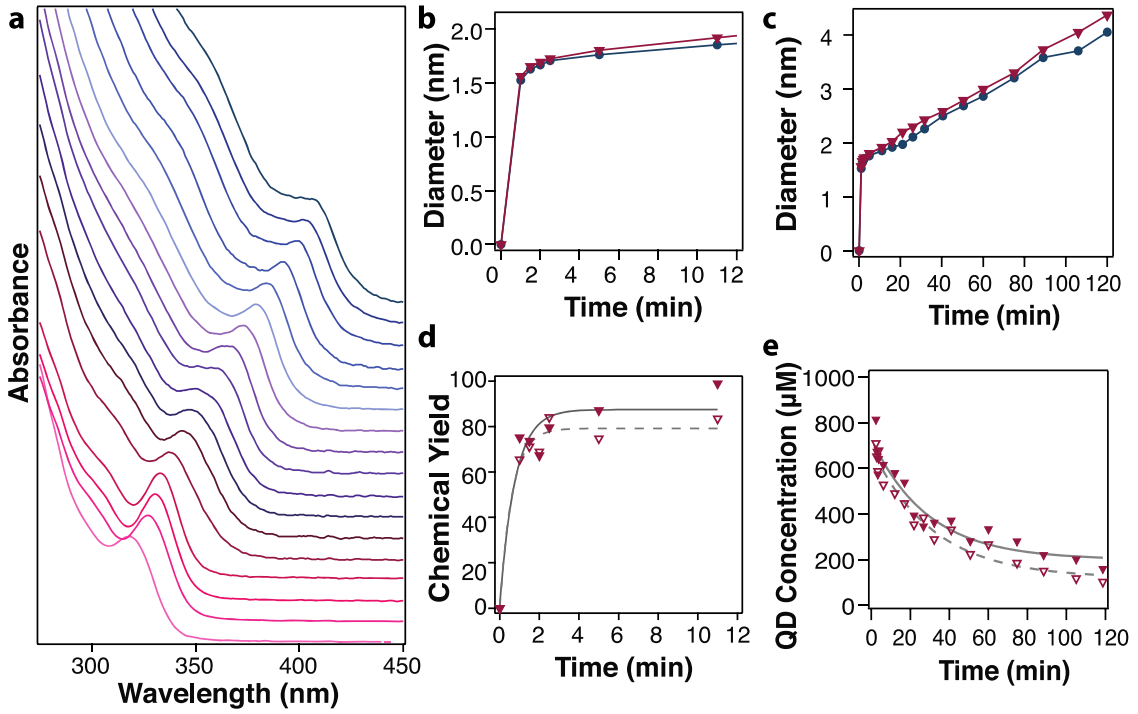


**Figure 6.** Using the fit equations to monitor a ZnSe QD synthesis reaction. (a) Spectra of QD samples taken from a single reaction started with a bolus hot injection followed by a slow drip of additional reactants. (b, c) Sizing of the QDs shown in panel (a) using either raw samples diluted in ODE for measurement on a NanoDrop pedestal (1 mm path length) with the 1S peak determined by manual examination of the absorbance intensities (blue circles) or raw samples diluted in hexane, measured in a cuvette (4 mm path length) with the lowest-energy transition determined using the second derivative of the spectrum (mauve triangles). Panel (b) is limited to the initial bolus hot-injection reaction, while panel (c) also shows the growth of the particles during the continuous drip phase of the reaction. (d) Chemical yield of the initial bolus injection calculated using the 1S peak intensity (hollow triangles) or integrated (solid triangles) molar extinction coefficients from eqs 6 and 7, respectively. Power law fits represented by dashed and solid lines, respectively, are used to guide the eye. (e) Concentration of the QD reaction solution determined using the 1S peak intensity (hollow triangles) or integration from the 1S peak to 500 nm (solid triangles) of sample absorption measurements taken after dilution in hexane.

solution, respectively. These quantities have already been determined for QD compositions including PbS, PbSe, InAs, and CdSe, and their relationship to bulk values was demonstrated.[15,17,37,40,41] Following previously published discussions,[42] we calculated the intrinsic absorption coefficient ($\mu_i$, $cm^{-1}$) spectra for each of our ZnSe samples. $\mu_i$ is also called the attenuation coefficient, which describes the distance that light can penetrate through the solution containing material i, i.e., ZnSe. $\mu_i$ can be experimentally derived from the absorbance spectra ($Abs$) of the sample and the volume fraction of the semiconductor material in solution determined from MP-AES ($f$) and path length of light through the sample ($L$, cm) using

$$\mu_i = \frac{\mathrm{Abs}\ \ln(10)}{fL} \tag{9}$$

and

$$f = C_{Zn}\frac{M_{ZnSe}}{M_{Zn}}\frac{1}{2\rho_{ZnSe}}\left(1 + \frac{1}{R_{Zn/Se}}\right) \tag{10}$$

where $C_{Zn}$ and $R_{Zn/Se}$ are the zinc weight concentration and zinc-to-selenium ratio (Table 1), respectively, $M_{ZnSe}$ and $M_{Zn}$ are the molar mass of zinc selenide and zinc, respectively, and $\rho_{ZnSe}$ is the density of ZnSe. When the absorbance spectrum for each of the ZnSe samples is combined with the MP-AES data to determine the wavelength-dependent intrinsic absorption coefficient, $\mu_i$, one can see the impact of quantum confinement on the intrinsic absorption near the band edge, as well as the convergence of the intrinsic absorption at high energies/low wavelengths (Figure 5a).

The theoretical $\mu_{i,th}$ is used as a comparator, as it represents the intrinsic absorption of the bulk semiconductor, and is calculated using wavelength ($\lambda$)-dependent optical constants, including the real ($n$) and imaginary ($k$) parts of the refractive index of ZnSe and the local field factor $f_{LF}$, as well as the refractive index of the surrounding medium ($n_s$)

$$\mu_{i,th} = \frac{4\pi n k |f_{LF}|^2}{n_s \lambda} \tag{11}$$

$$|f_{LF}|^2 = \frac{9n_s^4}{(n^2 - k^2 + 2n_s^2)^2 + 4(nk)^2} \tag{12}$$

The intrinsic absorption spectra for all 10 samples ($\mu_i$) are plotted with $\mu_{i,th}$, calculated using hexanes as the solvent ($n_s$ = 1.375) (Figure 5a). (*Note:* chloroform is often a preferred solvent for this analysis because it has an index of refraction that matches that of the surface ligand oleylamine ($n_{OLA}$ = 1.460), ensuring that there is no optical impact from the ligand corona. In this case, we chose hexane to extend the optical range of our analysis deeper into the UV.) Although the two smallest particles exhibit quantum confinement features in their spectra around 300 nm, all of the other spectra converge nicely with each other and the bulk $\mu_{i,th}$. As expected, the empirical $\mu_i$ values determined for each of the samples are size-


https://doi.org/10.1021/acs.chemmater.1c02501
Chem. Mater. 2021, 33, 7527−7536

independent, consistent with each other and the calculated intrinsic absorption coefficient from eq 11 (Figure 5b). These experimentally derived intrinsic absorption coefficients (Table S2) can be used to determine the volume fraction, and thus concentration, of Zn in an unknown sample (Note S1). Examination of the values at several specific wavelengths shows excellent agreement between the individual experimental values, the mean of the experimental values, and the theoretical value for the bulk intrinsic absorption coefficient (Figure 5b), although all wavelengths are not equally aligned. Because extending to higher-energy wavelengths does not ensure a monotonic improvement in the agreement between $\mu_{i,th}$ and $\mu_i$, an observation that has been made for other QD compositions as well,[42] it is important to experimentally evaluate the measurement wavelengths to choose the most effective values.

High-energy molar extinction coefficients ($\varepsilon_\lambda$, $M^{-1}cm^{-1}$) can be calculated for QDs with a known diameter ($D$, nm) using the intrinsic absorption coefficient at the same wavelength ($\mu_i$, $cm^{-1}$) and Avogadro's number ($N_A$, $mol^{-1}$) (note: $nm^3 = 10^{-24}$ L)

$$\varepsilon_\lambda = \frac{10^{-24}\pi D^3 N_A}{6\ln(10)}\mu_{i,\lambda} \tag{13}$$

When plotted, the molar extinction coefficients clearly increase for larger particles (Figure 5c) and scales with particle volume ($D^3$). The resulting fit equations

$$\varepsilon_{260} = 36\,700D^3 \tag{14}$$

$$\varepsilon_{280} = 23\,800D^3 \tag{15}$$

$$\varepsilon_{300} = 18\,200D^3 \tag{16}$$

provide a simple way to use the diameter in nm (as determined by eq 2) to generate the $\varepsilon_\lambda$ in $M^{-1}$ $cm^{-1}$, which can be used with the absorption spectra to calculate QD concentration using the Beer–Lambert law. We chose these wavelengths as the most effective for the high-energy molar extinction coefficient determination because there was congruence between the mean $\mu_i$ and $\mu_{i,th}$; it is practical to take absorbance measurements in this range in a number of solvents and cuvette materials (although we have only demonstrated this fit equation using hexane), and only the smallest particles of our size series were impacted by quantum confinement effects at these wavelengths and then minimally. Scaling the $\varepsilon_{280}$ to the 1S peak wavelength using the sample-specific absorption spectrum confirms the consistency of the different ways of calculating $\varepsilon$ values presented here (Figure S8, Note S2).

To test the applicability of these equations in monitoring a reaction in progress, we used the equations for the ZnSe diameter and molar extinction coefficient to determine the size of ZnSe particles, their concentration in the reaction solution, and the chemical yield of the initial nucleation reaction (Figure 6). A hot-injection reaction was used to nucleate the particles, and then growth was promoted by dripping additional Zn and Se precursors into the reaction solution over the course of 2 hours, creating a set of particle samples from the same reaction flask (Figure 6a). Within 1 min of the bolus injection, nucleation of the ZnSe particles was evident through the emergence of the characteristic quantum confinement-based absorption peak. The 1S peak shifted >10 nm between the first and second minutes of the reaction before the peak shifting slowed substantially, producing particles less than 2 nm in diameter (Figure 6b). This is consistent with the high reactivity of $Et_2Zn$ producing rapid nucleation and leaving nominal residual monomers in solution to promote ongoing growth. From 11 to 120 min, the particle diameters increase steadily as a solution of $Et_2Zn$ and TOP:Se was added dropwise to the reaction solution, providing a steady addition of monomers at subnucleation concentrations (Figure 6c). Sizing of the samples is very consistent regardless of whether the spectra were taken of samples diluted in hexane or ODE, using a small volume absorbance measurement or cuvette, and regardless of whether the 1S peak position was determined from local maxima of the spectrum or fitting the second derivative of the absorbance. The small differences in the red and blue data points in Figure 6b,c are primarily due to subtle differences in 1S peaks determined using the spectra directly or using the second derivative.

Using either the 1S peak absorbance intensity or the integrated absorbance (eqs 6 or 7, respectively) to determine the ZnSe concentration, and subsequently the amount of the reactants incorporated into the ZnSe particles, enables the estimation of the chemical yield of the reactions from absorbance measurements of the diluted raw reaction solutions. The values from either of the approaches are very similar, but the 1S peak intensity method underestimates the concentration of the samples with broader 1S peaks (Figure 6d). The plateau seen in the power law fit to either set of concentration values supports the notion that the precursors react rapidly and are substantially depleted within the first minutes of the reaction. When looking at the concentration of the particles over the duration of the reaction, the concentration steadily decreases as volume is added through the drip addition of the precursors, while repeated sampling reduces the number of QDs in the reaction flask overall (Figure 6e).

Notably, realistic values were attained across this sample set even though the early samples exhibit 1S peaks bluer than the initial measurement data used to generate the fit equations. This is a direct benefit of using fit equation formats that are physically consistent. Using the previously published fit equations beyond the initial range of the samples used to generate those fit equations yields nonsensical results (Figure S7). At later times, where the particle sizes are in the range used for both this and the previous study, the size and concentration values are in agreement. The small particles from the early time points confound the previously described sizing equation, however, and that incorrect diameter propagates the error to the molar extinction equation and concentration determination. Note that determining the concentration of the particles using high-energy absorption measurements would be inappropriate for this example of monitoring the reaction in progress, as the raw solution contains excess precursor and ligands that contribute to absorption at those wavelengths.

## CONCLUSIONS

Determination of the size and concentration of a QD sample from a simple optical measurement is a key function of any characterization or application effort using the nanoparticles. Access to a standard set of equations to use for these size and concentration determinations is critical for consistency and repeatability in nanotechnology. In this study, we establish these foundational equations for ZnSe QDs by synthesizing and characterizing a size series of ZnSe nanocrystals with 1S


https://doi.org/10.1021/acs.chemmater.1c02501
Chem. Mater. 2021, 33, 7527−7536

peaks between 361 and 422 nm. A head-to-head comparison of average diameters obtained using TEM and SAXS demonstrated the advantage of using mean diameters determined with SAXS to include data for very small particles. Empirical fit equations correlating the QD band gap, diameter, and molar extinction coefficient are reported, providing a standard set of equations that can be used by others in the field for the efficient and economical determination of ZnSe particle size and concentration. Further analysis of the data revealed the correlation of molar extinction coefficients with QD volume at high-energy wavelengths, providing a straightforward and size distribution-independent pathway to the accurate calculation of sample concentrations.

## MATERIALS AND METHODS

**Materials.** Tri-*n*-octylphosphine (TOP, 97%), selenium pellets (99.99%), 1 M diethyl zinc solution in hexanes, zinc stearate ($ZnSt_2$, purum, 10−12% Zn basis), hydrogen peroxide solution ($H_2O_2$, ≥30%, for trace analysis), and oleylamine (OLA, 70%, tech grade) were purchased from Sigma-Aldrich. 1-Octadecene (ODE, ≥90%, technical grade) was purchased from Alfa Aesar. Anhydrous ethanol, hexanes, and nitric acid ($HNO_3$, trace metal grade) were purchased from Fisher Scientific. Capillary wax and a hot wax pen for sealing quartz capillaries used in SAXS measurements were purchased from Hampton Research. Single-element selenium (10 000 μg/mL in 10% $HNO_3$) and zinc (10 000 μg/mL in 4% $HNO_3$) standard solutions were purchased from High-Purity Standards. (*Warning:* $Et_2Zn$ is pyrophoric, extremely reactive, and should be handled with extreme caution. Appropriate safety practices for the use of oxidizers ($H_2O_2$) and strong acids ($HNO_3$) should be observed. The safest order for the combination of $HNO_3$ and $H_2O_2$ is the addition of $HNO_3$ to $H_2O_2$.)

**Precursors.** A 1 M stock solution of selenium in TOP was synthesized by stirring 10 mmol of selenium pellets and 10 mL of TOP together on a hot plate heated to 80 °C until the selenium pellets were completely dissolved. A 0.4 M stock solution of $ZnSt_2$ in ODE was prepared by mixing 4 mmol of $ZnSt_2$ and 10 mL of ODE on a hot plate at 150 °C in an argon glovebox until a clear colorless solution was obtained. To prepare a 0.2 M stock solution of sulfur in OLA, 2 mmol of elemental sulfur and 10 mL of OLA in a 100 mL three-neck round-bottom flask were heated at 120 °C under vacuum for 2 hours with multiple argon backfill and evacuation cycles. The cooled solution was stored in an argon glovebox for future use.

**Synthesis of ZnSe Nanocrystals.** ZnSe nanocrystals were synthesized by modifying a previously reported method.[22] First, 8 mL of oleylamine in a 100 mL four-neck round-bottom flask was degassed at 85 °C for 30 min with multiple argon backfill and evacuation cycles. The temperature was increased to 300 °C, and a mixture of 0.5 mL of 1 M TOP:Se and 0.8 mL of TOP was added to the flask. Once the temperature stabilized at 300 °C, a mixture of 0.5 mL of 1 M $Et_2Zn$ in hexane and 0.8 mL of TOP was quickly injected. After 10 min, a mixture of 4 mL of ODE, 4 mL of TOP, 1.8 mL of 1 M TOP:Se, and 1.8 mL of 1 M $Et_2Zn$ in hexane was injected into the reaction using a stepper motor syringe pump at a rate of 2 mL/hour. For QD422, an additional dropwise injection using the same precursor volumes was performed. Once the desired 1S peak was reached, the reaction was stopped by cooling the flask to room temperature. All samples were stored in an argon-filled glovebox for future use. For reaction tracking, the procedure described above was followed but with a slow injection drip rate of 3 mL/hr. To collect samples during this reaction, a stopper was removed from the neck of the flask with a positive pressure argon flow minimizing the introduction of oxygen as ∼0.3 mL of the reaction solution was removed with a glass Pasteur pipette.

**QD Sample Preparation.** Samples of QDs were purified through precipitation and resuspension. QDs were diluted with a 1:1 volume ratio of hexane. The QDs were centrifuged at 22 000 rcf for 3 min to remove any aggregates. The solution was transferred to a clean tube, and ethanol was added until the solution became visibly turbid. The sample was centrifuged at 22 000 rcf for 5 min to precipitate the QDs. The clear supernatant was decanted, and the QD pellet was resuspended in hexanes for characterization. QDs used for elemental analysis were precipitated and resuspended a second time.

**Characterization.** Absorbance spectra of the primary set of samples were taken using a NanoDrop 2000 UV−vis spectrophotometer using cuvettes with a 1 cm path length, a 0.4 cm path length, or a 1 mm path length of the pedestal.

Transmission electron microscopy (TEM) images were acquired using FEI Osiris and JEOL 2100 LaB6 high-resolution microscopes operating at 200 kV. Each sample was precipitated using ethanol and resuspended in hexanes and drop-cast on a copper TEM grid, which was washed successively by hexane, ethanol, and DI water. The grid was then gently heated to evaporate any residual water. TEM images were sized manually using ImageJ by determining the area enclosed within an outline drawn around the particle and calculating the diameter assuming a spherical nanocrystal.

Small-angle X-ray scattering (SAXS) measurements were performed on solutions of as-synthesized QDs diluted in hexanes. The samples were injected into disposable quartz capillaries with a 1.5 mm diameter and sealed using a capillary wax applied using a battery-operated hot wax pen. Once cooled, the wax provides an airtight seal. Aliquots were analyzed using a Bruker N8 Horizon, with a Cu K$\alpha$ radiation at 50 kV and 1000 μA. Data analysis was performed on Bruker's DIFFRAC.SAXS software assuming a spherical particle shape with a log−normal size distribution.

X-ray diffraction (XRD) measurements were performed by depositing purified QDs on a low-background silicon substrate. The samples were measured on a Bruker D8 Discover system in powder diffraction mode with Cu K$\alpha$ radiation. Detection occurred with a 0.3 second integration per step at 0.0207−0.0225° steps.

To perform elemental analysis, calibration solutions of Zn and Se with concentrations of 1, 2, 4, 10, and 20 mg/L were prepared by diluting 10 000 μg/mL of standard solutions of Zn and Se in ultrapure water. The QDs were prepared using a digestion process modified from a previously published method.[38] Specifically, 400 μL of each sample was transferred to a 15 mL PTFE conical tube and the excess solvent was evaporated by pulling the vacuum on the tube for 15 min. Two hundred microliters of $H_2O_2$ was added to the sample, and the tube was sealed tightly and quickly. After 3 min, 200 μL of nitric acid was added to the mixture. The cap was tightly and quickly sealed, and the solution was allowed to digest for 15 min. The sample was diluted to a total volume of 2 mL using ultrapure water. The samples were run on an Agilent 4200 MP-AES, and the concentration of both Zn and Se ions was measured. For each QD size, two sets of solutions were digested and measured, and each measurement was performed with five replicates. Reported values are the averages of the 10 measurements.

## ASSOCIATED CONTENT

### Supporting Information

The Supporting Information is available free of charge at https://pubs.acs.org/doi/10.1021/acs.chemmater.1c02501.

TEM images and sizing histograms, SAXS analysis, MP-AES calibration curves, application of intrinsic absorption coefficients, confirmation of molar extinction coefficient self-consistency, and reaction tracking comparing equations (PDF)

## AUTHOR INFORMATION

### Corresponding Author

**Allison M. Dennis** − *Division of Materials Science and Engineering, Boston University, Boston, Massachusetts 02215, United States; Department of Biomedical Engineering, Boston University, Boston, Massachusetts 02215, United States;*



https://doi.org/10.1021/acs.chemmater.1c02501
*Chem. Mater.* 2021, 33, 7527−7536

orcid.org/0000-0001-5759-9905; Email: aldennis@bu.edu

## Authors

**Reyhaneh Toufanian** − *Division of Materials Science and Engineering, Boston University, Boston, Massachusetts 02215, United States*

**Xingjian Zhong** − *Department of Biomedical Engineering, Boston University, Boston, Massachusetts 02215, United States*

**Joshua C. Kays** − *Department of Biomedical Engineering, Boston University, Boston, Massachusetts 02215, United States*

**Alexander M. Saeboe** − *Division of Materials Science and Engineering, Boston University, Boston, Massachusetts 02215, United States*

Complete contact information is available at: https://pubs.acs.org/10.1021/acs.chemmater.1c02501

## Notes

The authors declare no competing financial interest.

## ■ ACKNOWLEDGMENTS

Research reported in this publication was supported by the National Institute of General Medical Sciences of the National Institutes of Health under award number R01GM129437. This work was performed, in part, at the Harvard University Center for Nanoscale Systems (CNS), a member of the National Nanotechnology Infrastructure Network (NNIN), which is supported by the National Science Foundation under NSF award number ECS-0335765. This work was also supported by NSF award number 1337471 for the Bruker N8 Horizon SAXS and Bruker D8 discovery, housed in the Materials Science and Engineering Core Research Facility at Boston University.

## ■ REFERENCES

(1) Shirasaki, Y.; Supran, G. J.; Bawendi, M. G.; Bulović, V. Emergence of Colloidal Quantum-Dot Light-Emitting Technologies. *Nat. Photonics* **2013**, *7*, 13−23.

(2) Yuan, Q.; Wang, T.; Yu, P.; Zhang, H.; Zhang, H.; Ji, W. A Review on the Electroluminescence Properties of Quantum-Dot Light-Emitting Diodes. *Org. Electron.* **2021**, *90*, No. 106086.

(3) Prodanov, M. F.; Vashchenko, V. V.; Srivastava, A. K. Progress toward Blue-Emitting (460−475 nm) Nanomaterials in Display Applications. *Nanophotonics* **2021**, *10*, 1801−1836.

(4) Chern, M.; Kays, J. C.; Bhuckory, S.; Dennis, A. M. Sensing with Photoluminescent Semiconductor Quantum Dots. *Methods Appl. Fluoresc.* **2019**, *7*, No. 012005.

(5) Bhuckory, S.; Kays, J. C.; Dennis, A. M. In Vivo Biosensing Using Resonance Energy Transfer. *Biosensors* **2019**, *9*, 76.

(6) Wagner, A. M.; Knipe, J. M.; Orive, G.; Pepas, N. A. Quantum Dots in Biomedical Applications. *Acta Biomater.* **2019**, *94*, 44−63.

(7) Ji, B.; Koley, S.; Slobodkin, I.; Remennik, S.; Banin, U. ZnSe/ZnS Core/Shell Quantum Dots with Superior Optical Properties through Thermodynamic Shell Growth. *Nano Lett.* **2020**, *20*, 2387−2395.

(8) Kim, T.; Kim, K. H.; Kim, S.; Choi, S. M.; Jang, H.; Seo, H. K.; Lee, H.; Chung, D. Y.; Jang, E. Efficient and Stable Blue Quantum Dot Light-Emitting Diode. *Nature* **2020**, *586*, 385−389.

(9) Ryowa, T.; Ishida, T.; Sakakibara, Y.; Kitano, K.; Ueda, M.; Izumi, M.; Ogura, Y.; Tanaka, M.; Nikata, S.; Watanabe, M.; Takasaki, M.; Itoh, T.; Miyanaga, A. High-Efficiency Quantum Dot Light-Emitting Diodes with Blue Cadmium-Free Quantum Dots. *J. Soc. Inf. Disp.* **2020**, *28*, 401−409.

(10) Jang, E. P.; Han, C. Y.; Lim, S. W.; Jo, J. H.; Jo, D. Y.; Lee, S. H.; Yoon, S. Y.; Yang, H. Synthesis of Alloyed ZnSeTe Quantum Dots as Bright, Color-Pure Blue Emitters. *ACS Appl. Mater. Interfaces* **2019**, *11*, 46062−46069.

(11) Li, K. Y.; Yang, L. S.; Cui, J. Y.; Li, S.; Li, G. Effect of Doping Mechanism on Photogenerated Carriers Behavior in Cu-Doped ZnSe/ZnS/L-Cys Core-Shell Quantum Dots. *AIP Adv.* **2019**, *9*, No. 115021.

(12) Acharya, S.; Sarkar, S.; Pradhan, N. Material Diffusion and Doping of Mn in Wurtzite ZnSe Nanorods. *J. Phys. Chem. C* **2013**, *117*, 6006−6012.

(13) Saeboe, A. M.; Nikiforov, A. Y.; Toufanian, R.; Kays, J. C.; Chern, M.; Casas, J. P.; Han, K.; Piryatinski, A.; Jones, D.; Dennis, A. M. Extending the Near-Infrared Emission Range of Indium Phosphide Quantum Dots for Multiplexed in Vivo Imaging. *Nano Lett.* **2021**, *21*, 3271−3279.

(14) Reiss, P.; Protière, M.; Li, L. Core/Shell Semiconductor Nanocrystals. *Small* **2009**, *5*, 154−168.

(15) Moreels, I.; Lambert, K.; De Muynck, D.; Vanhaecke, F.; Poelman, D.; Martins, J. C.; Allan, G.; Hens, Z. Composition and Size-Dependent Extinction Coefficient of Colloidal PbSe Quantum Dots. *Chem. Mater.* **2007**, *19*, 6101−6106.

(16) Yu, W. W.; Qu, L.; Guo, W.; Peng, X. Experimental Determination of the Extinction Coefficient of CdTe, CdSe, and CdS Nanocrystals. *Chem. Mater.* **2003**, *15*, 2854−2860.

(17) Moreels, I.; Lambert, K.; Smeets, D.; De Muynck, D.; Nollet, T.; Martins, J. C.; Vanhaecke, F.; Vantomme, A.; Delerue, C.; Allan, G.; Hens, Z. Size-Dependent Optical Properties of Colloidal PbS Quantum Dots. *ACS Nano* **2009**, *3*, 3023−3030.

(18) Lin, S.; Li, J.; Pu, C.; Lei, H.; Zhu, M.; Qin, H.; Peng, X. Surface and Intrinsic Contributions to Extinction Properties of ZnSe Quantum Dots. *Nano Res.* **2020**, *13*, 824−831.

(19) Chestnoy, N.; Hull, R.; Brus, L. E. Higher Excited Electronic States in Clusters of ZnSe, CdSe, and ZnS: Spin-Orbit, Vibronic, and Relaxation Phenomena. *J. Chem. Phys.* **1986**, *85*, 2237−2242.

(20) Yang, L.; Zhu, J.; Xiao, D. Microemulsion-Mediated Hydrothermal Synthesis of ZnSe and Fe-Doped ZnSe Quantum Dots with Different Luminescence Characteristics. *RSC Adv.* **2012**, *2*, 8179−8188.

(21) Yu, K.; Hrdina, A.; Zhang, X.; Ouyang, J.; Leek, D. M.; Wu, X.; Gong, M.; Wilkinson, D.; Li, C. Highly-Photoluminescent ZnSe Nanocrystals via a Non-Injection-Based Approach with Precursor Reactivity Elevated by a Secondary Phosphine. *Chem. Commun.* **2011**, *47*, 8811−8813.

(22) Acharya, K. P.; Nguyen, H. M.; Paulite, M.; Piryatinski, A.; Zhang, J.; Casson, J. L.; Xu, H.; Htoon, H.; Hollingsworth, J. A. Elucidation of Two Giants: Challenges to Thick-Shell Synthesis in CdSe/ZnSe and ZnSe/CdS Core/Shell Quantum Dots. *J. Am. Chem. Soc.* **2015**, *137*, 3755−3758.

(23) Vreeland, E. C.; Watt, J.; Schober, G. B.; Hance, B. G.; Austin, M. J.; Price, A. D.; Fellows, B. D.; Monson, T. C.; Hudak, N. S.; Maldonado-Camargo, L.; Bohorquez, A. C.; Rinaldi, C.; Huber, D. L. Enhanced Nanoparticle Size Control by Extending LaMer's Mechanism. *Chem. Mater.* **2015**, *27*, 6059−6066.

(24) Shen, H.; Wang, H.; Li, X.; Niu, J. Z.; Wang, H.; Chen, X.; Li, L. S. Phosphine-Free Synthesis of High Quality ZnSe, ZnSe/ZnS, and Cu-, Mn-Doped ZnSe Nanocrystals. *Dalton Trans.* **2009**, 10534−10540.

(25) Li, L. S.; Pradhan, N.; Wang, Y.; Peng, X. High Quality ZnSe and ZnS Nanocrystals Formed by Activating Zinc Carboxylate Precursors. *Nano Lett.* **2004**, *4*, 2261−2264.

(26) Jain, A.; Ong, S. P.; Hautier, G.; Chen, W.; Richards, W. D.; Dacek, S.; Cholia, S.; Gunter, D.; Skinner, D.; Ceder, G.; Persson, K. A. Commentary: The Materials Project: A materials genome approach to accelerating materials innovation. *APL Mater.* **2013**, *1*, No. 011002.

(27) Maes, J.; Castro, N.; De Nolf, K.; Walravens, W.; Abécassis, B.; Hens, Z. Size and Concentration Determination of Colloidal Nanocrystals by Small-Angle x-Ray Scattering. *Chem. Mater.* **2018**, *30*, 3952−3962.

(28) Borchert, H.; Shevchenko, E. V.; Robert, A.; Mekis, I.; Kornowski, A.; Grübel, G.; Weller, H. Determination of Nanocrystal Sizes: A Comparison of TEM, SAXS, and XRD Studies of Highly Monodisperse CoPt 3 Particles. *Langmuir* **2005**, *21*, 1931−1936.
(29) Weir, M. P.; Toolan, D. T. W.; Kilbride, R. C.; Penfold, N. J. W.; Washington, A. L.; King, S. M.; Xiao, J.; Zhang, Z.; Gray, V.; Dowland, S.; Winkel, J.; Greenham, N. C.; Friend, R. H.; Rao, A.; Ryan, A. J.; Jones, R. A. L. Ligand Shell Structure in Lead Sulfide-Oleic Acid Colloidal Quantum Dots Revealed by Small-Angle Scattering. *J. Phys. Chem. Lett.* **2019**, *10*, 4713−4719.
(30) Dorfs, D.; Salant, A.; Popov, I.; Banin, U. ZnSe Quantum Dots within CdS Nanorods: A Seeded-Growth Type-II System. *Small* **2008**, *4*, 1319−1323.
(31) Lad, A. D.; Kiran, P. P.; More, D.; Kumar, G. R.; Mahamuni, S. Two-Photon Absorption in ZnSe and ZnSeZnS Core/Shell Quantum Structures. *Appl. Phys. Lett.* **2008**, *92*, No. 043126.
(32) Hines, M. A.; Guyot-Sionnest, P. Bright UV-Blue Luminescent Colloidal ZnSe Nanocrystals. *J. Phys. Chem. B* **1998**, *102*, 3655−3657.
(33) Groeneveld, E.; Witteman, L.; Lefferts, M.; Ke, X.; Bals, S.; Van Tendeloo, G.; De Mello Donega, C. Tailoring ZnSe-CdSe Colloidal Quantum Dots via Cation Exchange: From Core/Shell to Alloy Nanocrystals. *ACS Nano* **2013**, *7*, 7913−7930.
(34) Li, J.; Wang, L. W. Band-Structure-Corrected Local Density Approximation Study of Semiconductor Quantum Dots and Wires. *Phys. Rev. B* **2005**, *72*, No. 125325.
(35) Reiss, P.; Quemard, G.; Carayon, S.; Bleuse, J.; Chandezon, F.; Pron, A. Luminescent ZnSe Nanocrystals of High Color Purity. *Mater. Chem. Phys.* **2004**, *84*, 10−13.
(36) Peters, J. L.; De Wit, J.; Vanmaekelbergh, D. Sizing Curve, Absorption Coefficient, Surface Chemistry, and Aliphatic Chain Structure of PbTe Nanocrystals. *Chem. Mater.* **2019**, *31*, 1672−1680.
(37) Jasieniak, J.; Smith, L.; van Embden, J.; Mulvaney, P.; Califano, M. Re-Examination of the Size-Dependent Absorption Properties of CdSe Quantum Dots. *J. Phys. Chem. C* **2009**, *113*, 19468−19474.
(38) Morrison, C.; Sun, H.; Yao, Y.; Loomis, R. A.; Buhro, W. E. Methods for the ICP-OES Analysis of Semiconductor Materials. *Chem. Mater.* **2020**, *32*, 1760−1768.
(39) Li, J.; Chen, J.; Shen, Y.; Peng, X. Extinction Coefficient per CdE (E = Se or S) Unit for Zinc-Blende CdE Nanocrystals. *Nano Res.* **2018**, *11*, 3991−4004.
(40) Leatherdale, C. A.; Woo, W.-K.; Mikulec, F. V.; Bawendi, M. G. On the Absorption Cross Section of CdSe Nanocrystal Quantum Dots. *J. Phys. Chem. B* **2002**, *106*, 7619−7622.
(41) Yu, P.; Beard, M. C.; Ellingson, R. J.; Ferrere, S.; Curtis, C.; Drexler, J.; Luiszer, F.; Nozik, A. J. Absorption Cross-Section and Related Optical Properties of Colloidal InAs Quantum Dots. *J. Phys. Chem. B* **2005**, *109*, 7084−7087.
(42) Karel Čapek, R.; Moreels, I.; Lambert, K.; De Muynck, D.; Zhao, Q.; Van Tomme, A.; Vanhaecke, F.; Hens, Z. Optical Properties of Zincblende Cadmium Selenide Quantum Dots. *J. Phys. Chem. C* **2010**, *114*, 6371−6376.


https://doi.org/10.1021/acs.chemmater.1c02501
*Chem. Mater.* 2021, 33, 7527−7536